Global Analysis of the Source and Detector Nonstandard Interactions Using the Short Baseline $\nu - e$ and $\overline{\nu} - e$ Scattering Data

Amir N. Khan*
School of Physics, Sun Yat-Sen University, Guangzhou, Guangdong 510275, China
(Dated: May 31, 2016)

We present a global analysis of the semileptonic and purely leptonic nonuniversal and flavor-changing nonstandard neutrino interactions in all the known short-baseline neutrino− and antineutrino−electron scattering experiments. The nonstandard effects at the source and at the detector can be more transparent in these experiments because of the negligibly small ratio between the baselines and the neutrino energies, which is not enough for the neutrinos to oscillate, and thus can be sensitive to the new physics at the both ends. We use data from two electron-neutrino electron scattering experiments and six electron-antineutrino electron scattering experiments and combine them to find the best fits on the nonstandard parameters using the source-only, detector-only analyses, and then find the interplay between the two cases. The bounds obtained in some cases are stronger and new, in some cases comparable to the current ones, and in the other cases weaker. For instance, the bound obtained from the interplay between the source and detector nonstandard physics on the nonstandard parameter ε_{ee}^{udL} at the source is much stronger and is comparable with the indirect bound, but the bounds on the parameters $\varepsilon_{\mu e}^{udL}$ and $\varepsilon_{\tau e}^{udL}$ are weaker in this study in comparison with the indirect bounds. We also find a global fit on the standard weak mixing angle $\sin^2\theta_W = 0.249 \pm 0.020$ with 2% improvement in its precision in comparison with the previous studies.

arXiv:1605.09284v1 [hep-ph] 30 May 2016

I. INTRODUCTION

The discovery of the long-sought neutrino mixing parameter θ_{13} in the short-baseline disappearance reactor neutrino oscillation experiments, Double Chooz, RENO and Daya Bay [1–3] has completed the list of the unknown mixing parameters of the neutrino oscillation theory. The goals of the ongoing series of medium-baseline reactor neutrino disappearance experiments, JUNO and RENO50 [4, 5], and the long-baseline accelerator neutrino appearance experiments, NOvA and DUNE [6, 7], as well as future neutrino factory experiments [8] are to measure the leptonic CP-violating phase, the only yet unknown parameter of the theory, which is highly favored for the matter-antimatter asymmetry of the Universe, to determine the correct ordering of the neutrino masses, normal or inverted, and to achieve high precision in the standard mixing parameters and the magnitudes of the mass-squared differences. The solar neutrino experiment, BOREXINO, has recently yielded for the first time the real-time measurement of the low-energy pp neutrinos [9] which, although not very precise, are a milestone for the solar neutrino flux. Concurrently, LENA is underway to give a high-precision measurement of the mixing parameters [10].

The short-baseline accelerator neutrino- and reactor antineutrino-electron elastic scattering experiments [11–17] have played a key role in confirming the gauge structure of standard model, in precisely testing the electroweak mixing parameter, $\sin^2\theta_W$, [11–17] and constraining the nonstandard physics parameters [18–25]. Though these experiments are very challenging because of the tiny sizes of cross sections, they are perfect probes of the precise determination of the $\sin^2\theta_W$ and the nonstandard physics because no complications due to the hadronic structure are involved. These experiments are also explored for hints on neutrino magnetic moments [22, 25], searches for unparticles [25], neutrino $Z^{'}$couplings [26], the large mass-squared difference case due to the sterile neutrinos [27] ($\sim$1eV^2) and the nonstandard neutrino interactions (NSIs).

The currently running precision neutrino oscillation and neutrino– and antineutrino-electron elastic scattering experiments can be used as perfect probes for the new physics due to the lepton universality violation and the lepton flavor violation. In the neutrino oscillation experiments, nonuniversal (NU) and flavor-changing (FC) NSIs are studied in combination with the neutrino oscillations at the neutrino source, propagation and at the detector [28–36]. On the other hand, in the short-baseline neutrino– and antineutrino-electron scattering experiments, these NSIs can be studied without the interference of neutrino oscillations because their baselines and energies result in small L/E$_\nu$ ratios and one can safely ignore the oscillation effects. Another important aspect of the NSI study in

*Electronic address: khan8@mail.sysu.edu.cn
ntrnphysics@gmail.com

the short-baseline experiments is that their measurements are independent of the energy resolution of the detector because the neutrino beam dispersion is negligibly small and there are no degeneracies between NSIs and the energy uncertainties of the beam [19–21]. As has been checked in Refs. [19–21] there are no effects of the energy resolution on the size of neutrino cross sections in these experiments, so we ignore the detector energy resolution effects for all the reactor neutrino cross sections included in this study.

We use the formalism developed in Ref. [23] and extend the analysis of reference [19], where only NU NSIs were considered, to find the global fits on all the possible NSI parameters (NU and FC) at source and detector and their interplays as we did in Ref. [23] only for the case of TEXONO experiment. The striking feature of the formalism developed in Ref. [23] is that it connects the physics at the source and at the detector. This enables one to explore the semileptonic NSIs at the source using the recoiled electron data of $\nu - e$ and $\overline{\nu} - e$ scattering processes. The combination of the $\nu - e$ scattering data and $\overline{\nu} - e$ scattering data can significantly improve the detector NSI parameter bounds as the $\nu - e$ scattering data are sensitive to the left-handed (LH) couplings, whereas the $\overline{\nu} - e$ scatterings are sensitive to the right-handed (RH) couplings. We focus on the leading order neutrino- and antineutrino interaction processes, calculate their cross sections in the form appropriate for these experiments and then fit the global data from these experiments with all the unknown NSI parameters relevant for the $\nu - e$ and $\overline{\nu} - e$ scatterings. This analysis is based on the combined data of accelerator-based neutrino sources in the energy range (7-50) MeVand the reactor neutrino sources in the energy range of (3-8) MeV in the respective leptonic scattering processes.

In the following section, we review the formalism being used in this analysis. We then turn to the global fitting analysis for the standard model parameter, $\sin^2\theta_W$, in Sec. II using the combined data of the eight scattering experiments. In Sec. III, we find the global fits on NSI parameters only at the sources, using the recoiled electron energy data; we call them the source-only parameters. In Sec. IV, we turn to the global fitting analysis of the NSI parameters only at the neutrino detectors and them the detector-only parameters, using the recoiled energy spectrum at the detector. In Sec. V, we find the interplay between the source-only and the detector-only NSI parameters using the global data. In Sec. VI, we conclude and summarize.

II. FORMALISM AND NOTATIONS

A. NSI effective Lagrangians at the source and detector

For the setup under consideration, the sources of neutrinos are the charged-current (CC) pion decays at the accelerators and, for antineutrinos, are the CC neutron beta decays at the reactors, while the target particles at the detectors are electrons and the contributions for the $\nu - e/\overline{\nu} - e$ scatterings come from both the CC and neutral currents (NC). Therefore, the effective four-fermion LH Lagrangians governing the CC semileptonic decays at both the accelerators and reactors [31, 37, 38] and the LH and RH effective four-fermion Lagrangians for the leptonic $\nu - e/\overline{\nu} - e$ scattering processes [37–41] at the detector are, respectively, given as

$$\mathcal{L}^s = \mathcal{L}^s_{NU} + \mathcal{L}^s_{FC} \tag{1}$$

$$\mathcal{L}^\ell = \mathcal{L}^\ell_{NU} + \mathcal{L}^\ell_{FC}, \tag{2}$$

where,

$$\mathcal{L}^s_{NU} = -2\sqrt{2}G_F \sum_\alpha (1+\varepsilon^{udL}_{\alpha\alpha})(\bar{l}_\alpha\gamma_\lambda P_L U_{\alpha a}\nu_a)(\bar{d}\gamma^\lambda P_L u)^\dagger + h.c., \tag{3}$$

$$\mathcal{L}^s_{FC} = -2\sqrt{2}G_F \sum_{\alpha\neq\beta} \varepsilon^{udL}_{\alpha\beta}(\bar{l}_\alpha\gamma_\lambda P_L U_{\beta a}\nu_a)(\bar{d}\gamma^\lambda P_L u)^\dagger + h.c., \tag{4}$$

$$\mathcal{L}^\ell_{NU} = -2\sqrt{2}G_F \sum_\alpha (\bar{e}\,\gamma_\mu\,(\widetilde{g}_{\alpha R}P_R + (\widetilde{g}_{\alpha L}+1)P_L)e)\,(\bar{\nu}_\alpha\gamma^\mu P_L\nu_\alpha), \tag{5}$$

$$\mathcal{L}^\ell_{FC} = -2\sqrt{2}G_F \sum_{\alpha\neq\beta} \varepsilon^{eP}_{\alpha\beta}(\bar{e}\gamma_\lambda Pe)(\bar{\nu}_\alpha\gamma^\lambda P_L\nu_\beta), \tag{6}$$

where

$$\widetilde{g}_{\alpha R} = \sin^2\theta_w + \varepsilon^{eR}_{\alpha\alpha} \text{ and } \widetilde{g}_{\alpha L} = \sin^2\theta_w - \frac{1}{2} + \varepsilon^{eL}_{\alpha\alpha}.$$

The superscripts "s" and "l" designate semileptonic and leptonic and the subscripts "NU" and "FC" correspond to the nonuniversal and flavor-changing NSIs for both the cases, respectively. Here "α" and "β" are the flavor-basis indices and "a" is the mass-basis index which can be eliminated by the effective replacement of $U_{\alpha a}\nu_a \to \nu_\alpha$ in Eq. (3) and $U_{\beta a}\nu_a \to \nu_\beta$ in Eq. (4), because oscillations play no role due to the small L/E_ν ratio for these experiments.

For simplicity, we consider only the LH effective Lagrangian at the sources and ignore the RH part because we do not consider any RH interactions of neutrinos in this study. The complex coefficients $\varepsilon^{udL}_{\alpha\beta}$ represent the relative coupling strengths of the flavor combinations in the presence of new physics at accelerator or reactor sources, and the complex coefficients $\varepsilon^{eP}_{\alpha\beta}$ represent the relative coupling strengths of the flavor combinations in the presence of new physics at detector to SM, while in the SM case both $\varepsilon^{udL}_{\alpha\beta} = 0$ and $\varepsilon^{eP}_{\alpha\beta} = 0$. The Hermiticity of the leptonic effective Lagrangian, L^ℓ, requires that the detector NSI parameters matrix is Hermitian and therefore, $\epsilon^{eR,L}_{\alpha\beta} = (\epsilon^{eR,L}_{\beta\alpha})^*$, so the NU NSI parameters at the detectors are real, but the FC NSI parameters are complex in general. With the effective Lagrangians defined, we are now ready to summarize the cross sections and flux factors needed for quantifying the NSI effects at the source and detector.

B. $\nu_e/\overline{\nu}_e - e$, $\nu_\mu/\overline{\nu}_\mu - e$ and $\nu_\tau/\overline{\nu}_\tau - e$ scattering cross sections

It is a well-known fact that the $\nu_e/\overline{\nu}_e - e$ scattering processes get contributions from both the NC and CC interactions, whereas the $\nu_\mu/\overline{\nu}_\mu - e$ and $\nu_\tau/\overline{\nu}_\tau - e$ scattering processes have contributions only coming from the NC interactions. Therefore, the $\nu_e/\overline{\nu}_e - e$ scattering cross sections are the coherent sums of the NC and CC contributions and the $\nu_\mu/\overline{\nu}_\mu - e$ and $\nu_\tau/\overline{\nu}_\tau - e$ scattering cross sections have only NC contributions. All the SM contributions are implicitly given in the definitions of the parameters $\widetilde{g}_{eL}$ and $\widetilde{g}_{eR}$ for the $\nu_e/\overline{\nu}_e - e$ scattering processes and those for $\nu_\mu/\overline{\nu}_\mu - e$ and $\nu_\tau/\overline{\nu}_\tau - e$ scattering processes are given in the definitions of $\widetilde{g}_{\mu L}$, $\widetilde{g}_{\mu R}$, $\widetilde{g}_{\tau L}$ and $\widetilde{g}_{\tau R}$. The differential cross sections for the three processes of $\nu_e - e$, $\nu_\mu - e$ and $\nu_\tau - e$ scatterings are given in a compact form as [23],

$$\begin{aligned}\left[\frac{d\sigma(\nu_\beta e)}{dT}\right]_{SM+NSI} &= \frac{2G_F^2 m_e}{\pi}\Big[\widetilde{g}^2_{\beta L} + \sum_{\alpha\neq\beta}|\varepsilon^{eL}_{\alpha\beta}|^2 \\ &+ \left((\widetilde{g}_{\beta R})^2 + \sum_{\alpha\neq\beta}|\varepsilon^{eR}_{\alpha\beta}|^2\right)\left(1-\frac{T}{E_\nu}\right)^2 \\ &- \left(\widetilde{g}_{\beta L}(\widetilde{g}_{eR}) + \sum_{\alpha\neq\beta}\Re[(\varepsilon^{eL}_{\alpha\beta})^*\varepsilon^{eR}_{\alpha\beta}]\right)\frac{m_e T}{E_\nu^2}\Big], \end{aligned} \tag{7}$$

where $\alpha,\ \beta = e,\mu,\tau$ and

$$\begin{aligned}\text{for } \beta &= e,\ \widetilde{g}_{\beta L} = \widetilde{g}_{eL} \text{ and } \widetilde{g}_{\beta R} = \widetilde{g}_{eR} + 1, \\ \text{for } \beta &= \mu,\ \widetilde{g}_{\beta L} = \widetilde{g}_{\mu L} \text{ and } \widetilde{g}_{\beta R} = \widetilde{g}_{\mu R}, \\ \text{for } \beta &= \tau,\ \widetilde{g}_{\beta L} = \widetilde{g}_{\tau L} \text{ and } \widetilde{g}_{\beta R} = \widetilde{g}_{\tau R}, \end{aligned} \tag{8}$$

and the differential cross sections of $\overline{\nu}_e - e$, $\overline{\nu}_\mu - e$ and $\overline{\nu}_\tau - e$ scatterings are

$$\begin{aligned}\left[\frac{d\sigma(\overline{\nu}_\beta e)}{dT}\right]_{SM+NSI} &= \frac{2G_F^2 m_e}{\pi}\Big[\widetilde{g}^2_{\beta R} + \sum_{\alpha\neq\beta}|\varepsilon^{eR}_{\alpha\beta}|^2 \\ &+ \left((\widetilde{g}_{\beta L})^2 + \sum_{\alpha\neq\beta}|\varepsilon^{eL}_{\alpha\beta}|^2\right)\left(1-\frac{T}{E_\nu}\right)^2 \\ &- \left(\widetilde{g}_{\beta R}(\widetilde{g}_{eL}) + \sum_{\alpha\neq\beta}\Re[(\varepsilon^{eR}_{\alpha\beta})^*\varepsilon^{eL}_{\alpha\beta}]\right)\frac{m_e T}{E_\nu^2}\Big], \end{aligned} \tag{9}$$

where $\alpha,\ \beta = e,\mu,\tau$ and

$$\begin{aligned}\text{for } \beta &= e,\ \widetilde{g}_{\beta L} = \widetilde{g}_{eL} + 1,\ \widetilde{g}_{\beta R} = \widetilde{g}_{eR} \\ \text{for } \beta &= \mu,\ \widetilde{g}_{\beta L} = \widetilde{g}_{\mu L},\quad \widetilde{g}_{\beta R} = \widetilde{g}_{\mu R} \\ \text{for } \beta &= \tau,\ \widetilde{g}_{\beta L} = \widetilde{g}_{\tau L},\quad \widetilde{g}_{\beta R} = \widetilde{g}_{\tau R} \end{aligned} \tag{10}$$

where Eq. (7) and (9) are the sums of the scattering cross sections for the three incoherent processes corresponding to each index of β. For instance, for $\nu_e - e$ scattering, it is the sum of $\nu_e + e \to \nu_e + e$, $\nu_e + e \to \nu_\mu + e$ and $\nu_e + e \to \nu_\tau + e$

Experiment	$E_\nu(MeV)$	T(MeV)	Events	Cross-Sections	$\sin^2\theta_W$
LSND	$20 < E_\nu < 50$	20-50	191	$[10.1 \pm 1.86]E_\nu \times 10^{-45}\text{cm}^2$	0.248 ± 0.051
LAMPF	$7 < E_\nu < 50$	7-50	236	$[10.1 \pm 1.74]E_\nu \times 10^{-45}\text{cm}^2$	0.249 ± 0.063
IRVINE I	$1.5 < E_\nu < 8$	1.5-3.0	381	$[0.87 \pm 0.25] \times \sigma_{V-A}$	0.29 ± 0.05
IRVINE II	$3.0 < E_\nu < 8.0$	3.0-4.5	77	$[1.70 \pm 0.44] \times \sigma_{V-A}$	0.29 ± 0.05
KRANOYARSK	$3.2 < E_\nu < 8.0$	3.2-5.2	N.A	$[4.5 \pm 2.4] \times 10^{-46}\text{cm}^2/\text{fission}$	$0.22^{+0.7}_{-0.8}$
MUNU	$0.7 < E_\nu < 8.0$	0.7-2.0	68	$[1.07 \pm 0.34] \times \text{events/day}$	$0.25 \pm 0.08^*$
ROVNO	$0.6 < E_\nu < 8.0$	0.6-2.0	41	$[1.26 \pm 0.62] \times 10^{-46}\text{cm}^2/\text{fission}$	$0.29 \pm 0.15^*$
TEXONO	$3.0 < E_\nu < 8.0$	3.0-8.0	414 ± 100	$[1.08 \pm 0.26] \times \sigma_{SM}$	0.251 ± 0.04
Global	-	-	-	-	0.249 ± 0.020

TABLE I: List of the accelerator and reactor short basline $\nu - e$ and $\bar{\nu} - e$ scattering experiments with their energy ranges (E_ν), recoiled electron energies (T), the total number of observed events, cross-sections and the correponding measured values $\sin^2\theta_W$. Notice that the entries with * in the last column are not provided by these experiments, but we find best fits of $\sin^2\theta_W$ with 1σ uncertainty using the data for MUNU and ROVNO as shown in Fig 2. All of the errors displayed here are the quadrature sum of the statistical and the systematic uncertainties. The last row shows the global best fit value of $\sin^2\theta_W$ with 1σ uncertainty.

and for $\bar{\nu}_e - e$ scattering it is the sum of $\bar{\nu}_e + e \to \bar{\nu}_e \to e$, $\bar{\nu}_e + e \to \bar{\nu}_\mu + e$ and $\bar{\nu}_e + e \to \bar{\nu}_\tau + e$; likewise, for $\nu_\mu/\bar{\nu}_\mu - e$ and $\nu_\tau/\bar{\nu}_\tau - e$ scattering processes. Defining the complex parameters $\varepsilon^{eL}_{\alpha e}$ and $\varepsilon^{eR}_{\alpha e}$ as $|\varepsilon^{eL}_{\alpha e}|\exp(i\phi^{eL}_{\alpha e})$ and $|\varepsilon^{eR}_{\alpha e}|\exp(i\phi^{eR}_{\alpha e})$, where $\alpha \neq e$, and $\phi^{eL}_{\alpha e}$ and $\phi^{eR}_{\alpha e}$ are the corresponding phases of the complex quantities, the interference terms in Eq. (7) and Eq. (9) can be written in a form, that takes into account the phase differences of the NSI parameters which have been ignored in the previous studies of Refs. [18–21, 24, 25], but were included for the TEXONO case in Ref. [23],

$$\Re[(\varepsilon^{eR}_{\alpha e})^*\varepsilon^{eL}_{\alpha e}] = |\varepsilon^{eR}_{\alpha e}||\varepsilon^{eL}_{\alpha e}|\cos(\Delta\phi), \tag{11}$$

where $\Delta\phi = \phi^{eL}_{\alpha e} - \phi^{eR}_{\alpha e}$ is the phase difference between the LH and RH FC NSI parameters at the detector. With this parametrization, the values of $|\varepsilon^{eR}_{\alpha e}|$ and $|\varepsilon^{eL}_{\alpha e}|$ are always positive and the sign of the term is controlled by $\cos(\Delta\phi)$.

The total cross section for each process will be to integrate over the recoiled electron energy for the full range of the incoming neutrino beam as given in Table I. The total cross section for each process then becomes

$$\begin{aligned}\left[\sigma(\nu_\beta e)\right]_{SM+NSI} &= \frac{2G_F^2 m_e E_\nu}{\pi}[\widetilde{g}^2_{\beta R} + \sum_{\alpha\neq\beta}|\varepsilon^{eR}_{\alpha\beta}|^2 \\ &+ \frac{1}{3}\left((\widetilde{g}_{\beta L})^2 + \sum_{\alpha\neq\beta}|\varepsilon^{eL}_{\alpha\beta}|^2\right) \\ &- \left(\widetilde{g}_{\beta R}(\widetilde{g}_{eL}) + \sum_{\alpha\neq\beta}\Re[(\varepsilon^{eR}_{\alpha\beta})^*\varepsilon^{eL}_{\alpha\beta}]\right)\frac{m_e}{2E_\nu}].\end{aligned} \tag{12}$$

In the case of antineutrinos, each total cross section is integration over the recoiled electron energy convoluted by the incoming neutrino spectrum, energy resolution of the detector, and the efficiency factor; therefore, the theoretically modeled or expected cross section for each process is,

$$\left[\sigma(\bar{\nu}_\beta e)\right]_{SM+NSI} = \int_{T^{\min}}^{T^{\max}} dT \int_{E_\nu^{\min}(T)}^{E_\nu^{\max}} \frac{d\sigma(\bar{\nu}_\beta e)}{dT} \times \frac{d\,\phi(E_\nu)}{dE_\nu}\, dE_\nu, \tag{13}$$

where $d\phi(E_\nu)/dE_\nu$ is the reactor antineutrino spectrum, given as $d\phi(E_\nu)/dE_\nu = \sum_{k=1}^{4} a_k\phi_k(E_\nu)$, where a_k are the abundances of each fission elements, ^{235}U, ^{239}Pu,^{241}Pu and ^{238}U and $\phi_k(E_\nu)$ is flux parametrization of each element and $E_\nu^{\min}(T)=0.5(T+\sqrt{T^2+2m_eT})$ and $E_\nu^{\max}(T)=8$ MeV [19, 42]. Notice that in Eq. (13), we do not put the efficiency factor explicitly but our calculation must take into account the efficiency factor where it is required, specially for the MUNU experiment. As has been checked in Refs. [19–21], there are no effects of the energy resolution on the size of neutrino cross sections in the short-baseline experiments, so we ignore the detector energy resolution effects in this study.

In case of the short-baseline accelerator and reactor antineutrino scattering experiments, the distance between the source and detector is of the order of a few tens of meters; therefore, oscillation effects which are proportional to

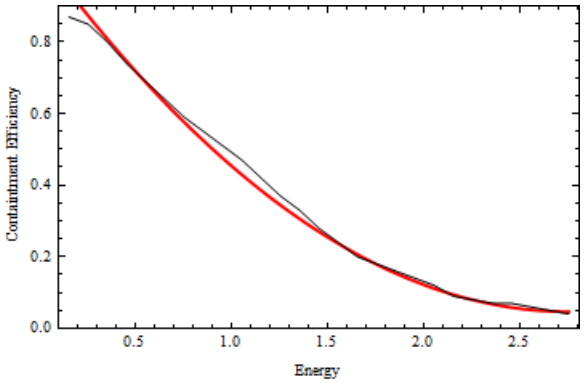

FIG. 1: Interpolation of the MUNU containment efficiency versus the antineutrino energy. The black curve is the continuum of the real data of the MUNU experiment. The red line is the fit to the data as defined by the function : 0.132382 (0.35 + (-2.75 + E_ν)^2)

the factor $\sin^2(m_i^2\text{-}m_j^2)L/4E_\nu$, are ignorable in case of the accelerator neutrinos (7MeV$\leq E_\nu \leq$50MeV) and the reactor neutrinos (3MeV$\leq E_\nu \leq$8MeV). Effectively, the neutrino flavor produced at the accelerator or reactor is the same as that at the detector. Therefore, only the NSI factors $\varepsilon_{\alpha\beta}^{udL}$ control flux of each neutrino flavor in the incoming beam to detector. Since the reactor neutrino flux model come out as a result of a large number of independent nuclear reactions and accelerator neutrino flux model is the result of a large number of pion decay reactions, so in the presence of NSIs, the emitted flux can be thought of as an incoherent sum of $\overline{\nu}_e, \overline{\nu}_\mu$ and $\overline{\nu}_\tau$ with weight factors $|1+\varepsilon_{ee}^{udL}|^2$, $|\varepsilon_{e\mu}^{udL}|^2$ and $|\varepsilon_{e\tau}^{udL}|^2$ and of ν_e, ν_μ and $\nu_\tau$with the same weights factors as for the case of reactor neutrinos. The source and detector NSI parameters can, therefore, be combined with each other through the factor $\mathcal{F}$ as

$$\mathcal{F}(\sin^2\theta_W,\ \varepsilon_{\alpha\beta}^{udL},\ \varepsilon_{\alpha\beta}^{eR},\ \varepsilon_{\alpha\beta}^{eL}) = \sum_{\alpha=e,\mu,\tau} |\delta_{e\alpha} + \varepsilon_{e\alpha}^{udL}|^2 \left[\sigma(\nu_\alpha e) + \sigma(\overline{\nu}_\alpha e)\right]_{SM+NSI}, \tag{14}$$

which is again the incoherent sum of the three cross sections for the $\nu_\alpha e-$scatterings and the three cross sections for the $\overline{\nu}_\alpha e-$scatterings as given in Eq. (12) and Eq. (13), respectively.

In case of the MUNU experiment, the available data is in the form of event rates. We have used the real data of the detector's containment efficiency to calculate the expected event rates, whereas the analysis of Ref. [19] is based on the assumption of including the normalization in the theoretical flux as the inverse of the efficiency. The containment efficiency of the detector versus the antineutrino energy is shown in Fig. 1, where the black curve is the interpolation of the real data points of the containment efficiency corresponding to the energy range (0.15-2.75) MeV, whereas red curve is the fit to the data with the fit function, $0.132382(0.35 + (-2.75 + E_\nu)^2)$. This function has been used to calculate the event rate as 1.07 ± 0.042 which is consistent with the one as quoted by the MUNU experiment [16].

C. The χ^2-fitting model

To fit the model to the combined data of the accelerator and reactor experiments and to minimize it for $\sin^2\theta_W$ and for the NSI parameters, we adopt the χ^2 definition from Refs. [19–23, 25] as

$$\chi^2 = \sum_i \left(\frac{\mathcal{F}_E^i - \mathcal{F}_X^i(\sin^2\theta_W, \varepsilon_{\alpha\beta}^{udL}, \varepsilon_{\alpha\beta}^{eR}, \varepsilon_{\alpha\beta}^{eL})}{\Delta^i} \right)^2, \tag{15}$$

where $\mathcal{F}_E^i$ and $\mathcal{F}_X^i$ are the experimental and expected factors which contain the SM and the NSI contribution of source and detector in the cross sections as defined in Eq. (14) for the ith experiment, and Δ^i represents the statistical and the systematic uncertainty of each experiment added in the quadrature. Since we are using final cross sections and their total uncertainties from different experiments as the input data points and each datum is a result of an

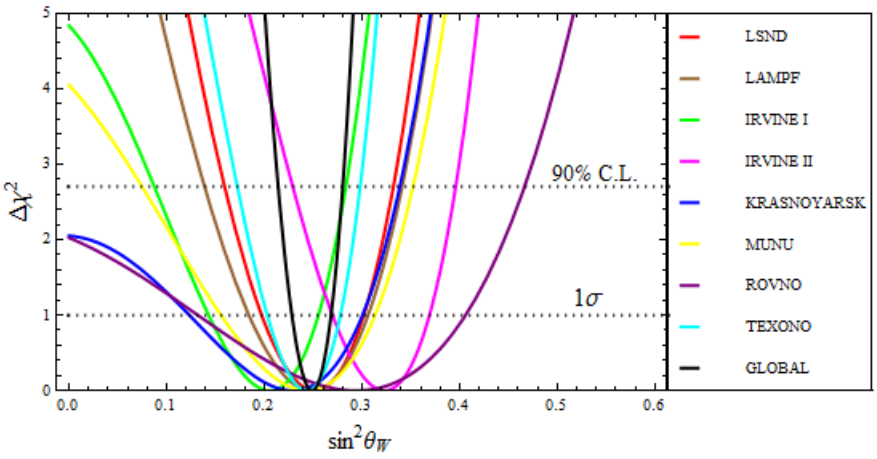

FIG. 2: Best fits of $\sin^2\theta_W$ from the individual short-baseline accelerator neutrino and reactor antineutrino experiments and their global $\Delta\chi^2$ fit. Each experimental fit can be identified by the corresponding legend color as assigned in the vertical table on the right side. The dotted horizontal lower and upper lines corresponding to the 1σ and 90% C.L. are shown for guidance. The global fit corresponds to the black curve.

extensive statistical analysis, the total uncertainty can be considered as the statistical fluctuation of each datum in the global analysis like in the case of the standard χ^2 definition used for a single experiment's data points.

We present our analysis for the SM case in terms of $\Delta\chi^2$ versus $\sin^2\theta_W$, where $\Delta\chi^2 = \chi^2 - \chi^2_{\rm min}$, for each individual experiment and for the case of global fit. Similarly, in the case of the minimization of the χ^2 function for NSI parameters we consider the two-parameter fits using the $\Delta\chi^2$ versus two NSI parameters each. For this purpose we define $\Delta\chi^2 = \chi^2 - \chi^2_{\rm min}$, where $\Delta\chi^2$ is taken to be 2.71, 3.84 and 6.63 corresponding to the 90%, 95%, and 99% confidence levels (C.L.). This is different from Ref. [19], where the two parameter values of $\Delta\chi^2$ were added with the $\chi^2_{\rm min}$ to get their bounds from 1 parameter projection of the 90% C.L. contour boundaries.

III. GLOBAL FITS OF $\sin^2\theta_W$, SOURCE AND DETECTOR NSI PARAMETERS INDEPENDENTLY

In this section, we repeat the analysis of Sec. III of Ref. [23] using the combined data of the reactor- and accelerator -based leptonic scattering experiments as listed in Table I. We include the FC NSI effects in the work done in Ref. [19], where only the NU NSIs have been considered. We further explore the NSI phase effects due the FC NSI parameters at the detector using the combined data, which has been studied before in Ref. [23] only for the case of the TEXONO experiment [17, 25].

A. Standard model fits

Using the definition of χ^2 in Eq. (15), we minimize it to obtain the best fit for $\sin^2\theta_W$ using the combined experimental data as given in Table I. All the NSI parameters are set equal to zero for this fitting. We have added IRVIVE II and the TEXONO to the list of experiments as taken for the same analysis in Ref. [22]. The χ^2-minima and the best-fits for each experiment and the global minimum and the related best fit value are all shown in Fig. 2. Each experimental input is identified by a particular color assigned in the legend aside. The black curve shows the global best fit with a value of $\sin^2\theta_W = 0.249 \pm 0.020$ at minimum-χ^2 of 2.68. The uncertainty shown is 1σ when the minimum-$\Delta\chi^2 = 0$, a better fit than the one obtained in Ref. [22] having precision of 10% at 1σ, whereas in our case we have precision of 8%. The 1σ and 90% C.L. lines are included for guidance in Fig. 2.

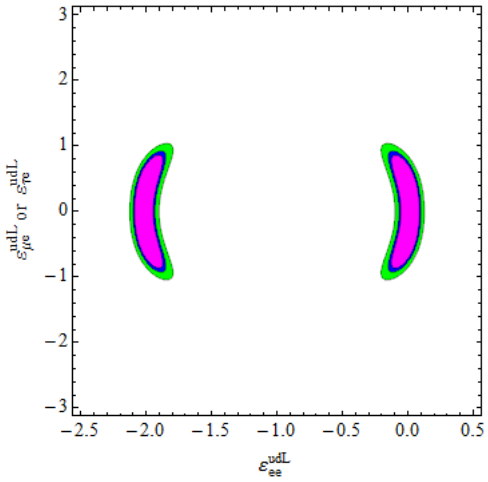

FIG. 3: Global analysis for the source-only NSI parameters case. The three different contour regions correspond to the 90%, 95% and 99% C.L. from inner to outer, respectively.

B. NSIs with the Source-Only Case

Here we present the analysis for the source-only (semileptonic) NSI parameters using the combined data of the accelerator and reactor experiments as listed in Table I. As discussed in Sec. I, although we are using the data from the recoiled electron energy spectrum at the detector, our formalism still allows us to obtain constraints on the source-only NSI parameters. We take contour boundaries of the source-only NSI parameters in the $(\mathrm{NU}(\varepsilon_{ee}^{udL})-\mathrm{FC}(\varepsilon_{\alpha e}^{udL}))$ parameter space and then extract bounds from the projections on the relevant axes as shown in Fig. 3. The figure shows the boundaries of the two-parameter fits to the combined data of the experiments at a 90%, 95%, and 99% C.L. boundaries as colored as red (inner), blue (middle) and green (outer), respectively. The bounds obtained from the contours corresponding to the 90% C.L. are given in the first two rows of Table II.

C. NSIs with the Detector-Only Case and the NSI Phase Effects

A similar exercise, as in Sec. IIIB, is repeated for the detector-only (leptonic) NSI parameters and the results are shown in Fig. 4, where Fig. 4(a) shows the contour boundaries of the detector-only NU NSI parameters and the other three panels show the contours of the detector FC NSI parameters at 90%, 95%, and 99% C.L.. Figs. (4(b)-4(d)) show effects of the NSI phase, appearing in the RH-LH interference term of Eq. (7) and Eq. (9) on the C.L. boundaries, when the NSI phases have values $\cos(\Delta\phi) = 1, 0$ and -1, which is coming from the RH-LH interference terms of the FC NSI parameters at the detector in the differential cross sections. Each choice of the phase part corresponds to the different choices of the NSI phases and their differences. For example, Fig. 4(d) corresponds to the composite of the cases $\phi_{\alpha e}^{eR} = \phi_{\alpha e}^{eL} = 0$, where $\epsilon_{\alpha e}^{eR}$ and $\epsilon_{\alpha e}^{eL}$ are both real and positive, $\phi_{\alpha e}^{eR} = \pi$ and $\phi_{\alpha e}^{eL} = 0$, where $\epsilon_{\alpha e}^{eR}$ is real and negative and $\epsilon_{\alpha e}^{eL}$ is real and positive, $\phi_{\alpha e}^{eR} = \phi_{\alpha e}^{eL} = \pi$, where $\epsilon_{\alpha e}^{eR}$ and $\epsilon_{\alpha e}^{eL}$ are both real and negative, and, finally, $\phi_{\alpha e}^{eR} = 0$ and $\phi_{\alpha e}^{eL} = \pi$, where $\epsilon_{\alpha e}^{eR}$ is real and positive and $\epsilon_{\alpha e}^{eL}$ is real and negative. Alternatively, it can be interpreted as the composite of cases where 0 and π are replaced with $\pi/2$ and $3\pi/2$ and the real is replaced with the imaginary. Similarly, Fig. 4(c) corresponds to those composite choices in which $\phi_{\alpha e}^{eL} - \phi_{\alpha e}^{eR} = \pi/2$. For such choices the correlation between the RH and LH FC NSI parameters appearing the LH-RH interference term disappears, because RH and LH parameters are $\pi/2$ out of phase; for example, one can be real and the other can be imaginary.

It is clear from Eq. (7) and (9), the RH-LH interference term of the FC NSI parameters are suppressed by the factor $m_e T/E_\nu^2$, where the mean of the lower end of the neutrino energies listed in the Table I is greater than 6.5 MeV and effects of the phases are thus very small, as shown in Figs. 4(b), 4(c) and 4(d). Conclusions about allowed boundaries for NSI parameters for the range of energies of interest in the combined accelerator and reactor short-baseline experiment are affected very little in this analysis, but for experiments with significantly lower energy radioactive sources or for low-energy solar neutrinos such as those coming from pp, ^{7}Be, and B^8 reactions, and marginally for the lower end of the pep spectrum, which are all measured in Gallium [43] and BOREXINO [44]

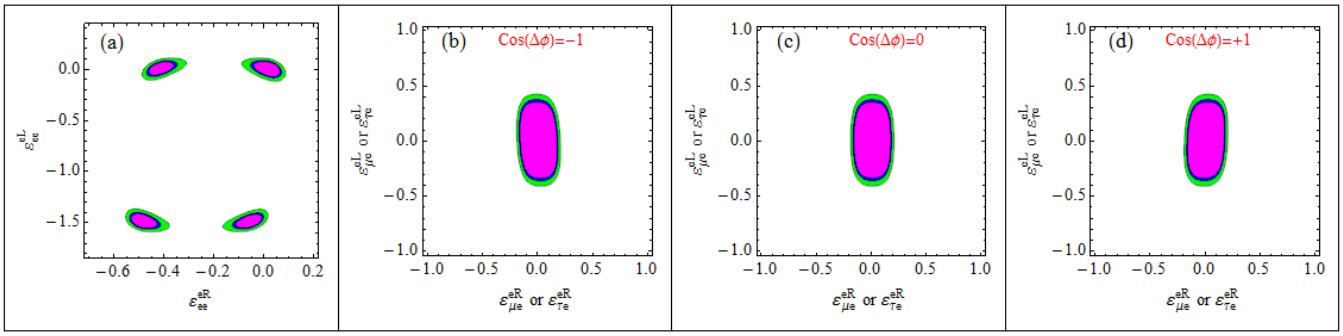

FIG. 4: Global analysis for the detector-only NSI parameters case. In each panel, the three different contour regions correspond to the 90%, 95%, and 99% C.L. from inner to outer, respectively. Panel (a) shows the NU NSI parameter boundary regions, whereas (b) corresponds to $\cos(\Delta\phi) = -1$, (c) to $\cos(\Delta\phi) = 0$ and (d) corresponds to $\cos(\Delta\phi) = +1$ of the FC NSI parameter boundary regions.

Figure No.	RH-Parameter Bounds	LH-Parameter Bounds
3	–	$-0.13 < \varepsilon_{ee}^{udL} < 0.10$
3	–	$-0.84 < \varepsilon_{\alpha e}^{udL} < 0.84$
$4(a)$	$-0.04 < \varepsilon_{ee}^{eR} < 0.06$	$-0.08 < \varepsilon_{ee}^{eL} < 0.08$
$4(b), \cos(\Delta\phi) = -1$	$-0.17 < \varepsilon_{\alpha e}^{eR} < 0.18$	$-0.33 < \varepsilon_{\alpha e}^{eL} < 0.35$
$4(c), \cos(\Delta\phi) = 0$	$-0.15 < \varepsilon_{\alpha e}^{eR} < 0.16$	$-0.33 < \varepsilon_{\alpha e}^{eL} < 0.35$
$4(d), \cos(\Delta\phi) = +1$	$-0.16 < \varepsilon_{\alpha e}^{eR} < 0.17$	$-0.33 < \varepsilon_{\alpha e}^{eL} < 0.35$

TABLE II: Bounds at 90% C.L. obtained from Fig. 3 for the source-only and from Fig. 4 for the detector-only case where $\alpha = \mu$ or τ.

experiments, the RH-LH correlation term can be relatively larger and the phase effects must become important.

IV. CORRELATION BETWEEN THE SOURCE AND DETECTOR NSI PARAMETERS

This section is a recap of section IV of Ref. [23] using the combined data of the short-baseline accelerator and reactor $\nu_e - e$ and $\overline{\nu}_e - e$ scattering experiments. Here the joint two- parameters C.L. boundary regions are taken where one is the source semileptonic NSI parameter and the other is the detector leptonic NSI parameter. First, we check the boundaries for the NU source versus all the detector NSI parameters and then FC source versus all the detector NSI parameters. Bounds are extracted for each parameter using its projection on the corresponding axis at 90% C.L..

A. The NU source (ε_{ee}^{udL}) versus all the detector ($\epsilon_{\alpha\beta}^{eR,\,L}$) NSI cases

We take pairs of NU source and all of the detector NSI parameters to survey the 90%, 95%, and the 99% C.L. boundaries in the two-parameter spaces. Only bounds at 90% C.L. are extracted and are displayed in Table III. The results of this analysis are displayed in Fig. 5 showing the C.L. boundaries for the fits to the combined data of the accelerator and reactor short-baseline scattering data parametrized by one source NSI parameter and one detector parameter with all of the other NSI parameters set to zero. From Fig. 5, we can determine the 90% C.L. bounds on the source NU parameter, ε_{ee}^{udL}, and on any of the detector NSI parameters, $\epsilon_{\alpha e}^{eR,L}$, where $\alpha = e,\ \mu,\ \tau$, by projecting onto the parameter axis for each contour. All of the extracted limits are given in Table III.

B. The FC source ($\varepsilon_{e\mu}^{udL}$ or $\varepsilon_{e\tau}^{udL}$) versus all the detector ($\epsilon_{\alpha\beta}^{eR,\,L}$) NSI cases

Here we present the interplay between the source FC NSI parameters and all of the corresponding detector NSI parameters (both NU and FC) and find the C.L. boundary regions at 90%, 95%, and 99% C.L. as shown in Fig. 6.

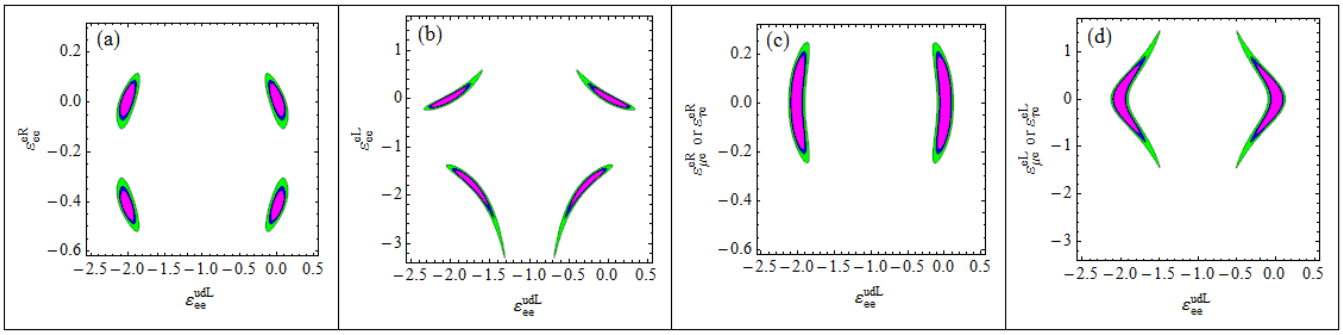

FIG. 5: Global analysis for the interplay between the source and detector NSI parameters. The three different contour regions in each panel correspond to the 90%, 95% and 99% C.L. from inner to outer, respectively.

Figure No.	NSI Parameters at Source	NSI Parameters at Detector
$5(a)$	$-0.09 < \varepsilon_{ee}^{udL} < 0.10$	$-0.06 < \varepsilon_{ee}^{eR} < 0.07$
$5(b)$	$-0.19 < \varepsilon_{ee}^{udL} < 0.25$	$-0.17 < \varepsilon_{ee}^{eL} < 0.23$
$5(c)$	$-0.09 < \varepsilon_{ee}^{udL} < 0.09$	$-0.19 < \varepsilon_{\alpha e}^{eR} < 0.19$
$5(d)$	$-0.25 < \varepsilon_{ee}^{udL} < 0.09$	$-0.73 < \varepsilon_{\alpha e}^{eL} < 0.75$

TABLE III: Bounds at 90% C.L. obtained from Fig. 5 for the NU source (ε_{ee}^{udL}) versus all the detector ($\epsilon_{\alpha\beta}^{eR,\,L}$) NSIs case where $\alpha, \beta = \mu, \tau$.

The bounds are extracted from the 90% C.L. boundaries and are given in Table IV. In this case only the bounds on the source NSI parameters, $\varepsilon_{e\mu}^{udL}$, can be extracted while detector NSI parameters, $\epsilon_{\alpha\beta}^{eR,L}$, remain unbounded. This is because the source is receiving $\bar{\nu}_e$ flux in the limit when $\varepsilon_{\alpha\beta}^{udL} \to 0$. This shows that the source NSI parameters, $\varepsilon_{\alpha\beta}^{udL}$, and detector NSI parameters, $\epsilon_{\alpha\beta}^{eR,L}$, are highly correlated. One can see that there is still a possibility for placing upper bounds on source NSI parameters, $\varepsilon_{e\alpha}^{udL}$, at 90% C.L. when the detector NSI parameters, $\epsilon_{\mu\mu}^{eR,\,L}$and $\epsilon_{\alpha\mu}^{eR,\,L}$, are zero , and likewise for $\mu \to \tau$. These are the so-called one-parameter-at-a-time bounds on the source NSI parameters commonly reported in the literature. The possible one-parameter-at-a-time bounds are given as asterisk entries in the 3rd column of Table V. We can see from Fig. 6 that in the case of FC source NSI parameters, there is no dependence on the detector NSI phase, because the phase effects are coming from the interference between the LH and RH parameters of the detector NSIs, but in this case the LH and RH parameters' contribution is coming separately in the two-parameters analysis; therefore, these results are not sensitive to the detector NSI phases.

Summarizing this section we can notice from the Tables III and IV that the bounds obtained from the two-

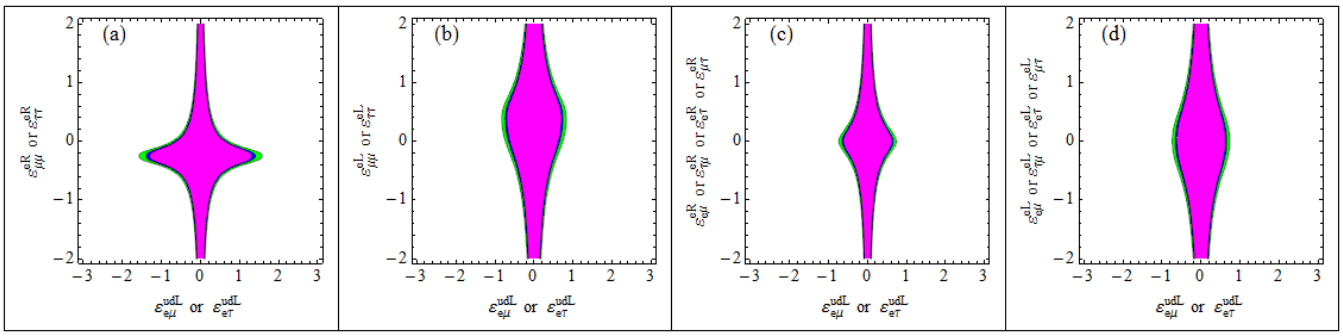

FIG. 6: C.L. boundaries for the correlation between the source FC NSI and all the detector (NU and FC) NSI parameters using the combined data of the very short baseline accelerator and reactor neutrino data at 90%, 95% and 99% C.L. The red, blue and green colors correspond to the three C.L. regions, respectively.

Figure no.	NSI parameters at Source	NSI parameters at detector
$6(a)$	$-1.3 < \varepsilon_{\alpha e}^{udL} < 1.3$	*unbounded*
$6(b)$	$-0.70 < \varepsilon_{\alpha e}^{udL} < 0.70$	*unbounded*
$6(c)$	$-0.62 < \varepsilon_{\alpha e}^{udL} < 0.62$	*unbounded*
$6(d)$	$-0.62 < \varepsilon_{\alpha e}^{udL} < 0.62$	*unbounded*

TABLE IV: Bounds at 90% C.L. obtained from Fig. (6) for the FC source ($\varepsilon_{e\mu}^{udL}$ or $\varepsilon_{e\tau}^{udL}$) versus all the detector ($\epsilon_{\alpha\beta}^{eR,\,L}$) NSI cases where $\alpha = \mu, \tau$.

parameter analysis of the same handedness are weaker, but the bounds with opposite handedness are stronger.

V. SUMMARY AND CONCLUSIONS

We have extended the work of Refs. [19, 22] by applying the formalism developed in Ref. [23] using the data of all the available accelerator and reactor neutrino scattering experiments, as listed in Table I, to find the global fit of the weak mixing parameter, $\sin^2\theta_W$, and to constrain the NU and FC NSI parameters, along with the NSI phase effects at the detector. The formalism developed in Ref. [23] can combine the NSI effects in the semileptonic decays at the accelerator and reactor neutrinos sources with the leptonic NSI effects at the detector. This formalism helps to find the sensitivity of the source NSIs using the detector data of the recoiled electrons. In addition, we can find the correlation between the source and detector NSI parameters.

We have first used the leptonic scattering data of the accelerator and reactor experiments to find the best-fit value of $\sin^2\theta_W$, as done before in Ref. [22], with the additional data set from the recent TEXONO experiment [17] added here. These combined data were then used to explore the NSIs at source and at the detector. We used the two-parameter joint C.L. boundaries for constraining the source and detector NSI parameters separately and then found the interplay between them.

In the case of $\sin^2\theta_W$, we find the minimum-χ^2 of $\chi^2_{\rm min}/{\rm d.o.f} = 2.68/7$. The results are consistent with the analysis when one experiment is excluded and the whole exercise is repeated for one experiment fewer than the total. We find a global best fit value of $\sin^2\theta_W = 0.249 \pm 0.020$ at 1σ with 8% precision, which is a 2% improvement in the previous value of $\sin^2\theta_W = 0.259 \pm 0.025$ at $\chi^2_{\rm min}/{\rm d.o.f} = 2.17/6$ of Ref. [22].

For the NSI case, we first used the model for the combined data when only the source semileptonic NSI parameters were considered while all the detector NSIs were set to zero. The joint two-parameter analysis between the source NU and the source FC NSIs were performed as shown in Fig. 3 and the corresponding bounds were obtained as given in Table II, and in the first three entries of Table V for comparison with previous bounds of Ref. [20, 21] and with the indirect bounds of Ref. [30]. As clear from Table V, the bound on the NU source parameter , ε_{ee}^{udL}, in the case of the correlated analysis is much stronger and is comparable with the bounds from the indirect study of the fourth column in the table. Similarly the source FC NSI parameters, $\varepsilon_{\mu e}^{udL}$ and $\varepsilon_{\tau e}^{udL}$, are weaker in this study in comparison with the indirect bounds, but are new in the sense that these have been obtained using the recoiled electron data at the detector. As shown in Ref. [23], improvement in the statistical uncertainty of the TEXONO experiment and use of this framework can improve the source NSI bounds in the scattering experiments. Similarly, the bounds obtained from the global data can also be improved.

In the case of detector-only NSIs, we performed the two-parameter best-fit analysis and have shown our results in Fig. 4 and the bounds obtained in Table II. The LH NU NSI parameter, ε_{ee}^{eL}, at the detector has a new stringent lower bounds with an order of magnitude improvement from the one previously obtained using a similar analysis. Since the FC parameters at the detector also contain the NSI phase contributions, we show them in three different panels in Fig. 4. Although the NSI phases do not have significant effects on the boundaries of the NSI parameters space, however they could have significant effects in the low energy experiments as has been shown in Ref. [23] in the section of future prospect study of TEXONO experiment.

In the last section, a correlation between the source semileptonic and the detector purely leptonic NSI parameters has been explored. The C.L. boundaries and the bounds obtained from them are given in Figs. 5 and 6 and in Tables III and IV. In Sec. IVA, we explore the interplay between the source NU NSI parameter, ε_{ee}^{udL}, versus all the detector NSI parameters, $\epsilon_{\alpha\beta}^{eR,\,L}$, whereas Sec. IVB deals with the interplay between the source FC NSIs, $\varepsilon_{e\mu}^{udL}$ or $\varepsilon_{e\tau}^{udL}$, versus all the detector NSI parameters, $\epsilon_{\alpha\beta}^{eR,\,L}$.

NSI parameters	This work (uncorrelated)	This work (correlated)	Previous bounds	M.I.Bs
ε_{ee}^{udL}	$-0.13 < \varepsilon_{ee}^{udL} < 0.10$	$-0.09 < \varepsilon_{ee}^{udL} < 0.09$	–	< 0.042
$\varepsilon_{\mu e}^{udL}$	$-0.84 < \varepsilon_{\mu e}^{udL} < 0.84$	$-0.62 < \varepsilon_{\mu e}^{udL} < 0.62^{*}$	–	< 0.042
$\varepsilon_{\tau e}^{udL}$	$-0.84 < \varepsilon_{\tau e}^{udL} < 0.84$	$-0.62 < \varepsilon_{\tau e}^{udL} < 0.62^{*}$	–	< 0.042
ε_{ee}^{eL}	$-0.08 < \varepsilon_{ee}^{eL} < 0.08$,	$-0.17 < \varepsilon_{ee}^{eL} < 0.23$	$-0.13 < \varepsilon_{ee}^{eL} < 0.12$	< 0.06
ε_{ee}^{eR}	$-0.04 < \varepsilon_{ee}^{eR} < 0.06$	$-0.06 < \varepsilon_{ee}^{eR} < 0.07$	$-0.07 < \varepsilon_{ee}^{eR} < 0.15$	< 0.14
$\varepsilon_{\mu e}^{eL}$	$-0.33 < \varepsilon_{\mu e}^{eL} < 0.35$	$-0.73 < \varepsilon_{\mu e}^{eL} < 0.75$	$-0.43 < \varepsilon_{\mu e}^{eL} < 0.43$	< 0.10
$\varepsilon_{\mu e}^{eR}$	$-0.15 < \varepsilon_{\mu e}^{eR} < 0.16$	$-0.19 < \varepsilon_{\mu e}^{eR} < 0.19$	$-0.31 < \varepsilon_{\mu e}^{eR} < 0.31$	< 0.10
$\varepsilon_{\tau e}^{eL}$	$-0.33 < \varepsilon_{\tau e}^{eL} < 0.35$	$-0.73 < \varepsilon_{\tau e}^{eL} < 0.75$	$-0.43 < \varepsilon_{\tau e}^{eL} < 0.43$	< 0.40
$\varepsilon_{\tau e}^{eR}$	$-0.15 < \varepsilon_{\tau e}^{eR} < 0.16$	$-0.19 < \varepsilon_{\tau e}^{eR} < 0.19$	$-0.31 < \varepsilon_{\tau e}^{eR} < 0.31$	< 0.27

TABLE V: Bounds for comparison of the model independent study of Ref. [30]. The asterisk entries correspond to the one-parameter-at-a-time bounds. Bounds of fourth column with the title "previous bounds" have been taken from Refs. [19–22], which uses analysis similar to this work. M.I.Bs refer to the model independent or indirect bounds and have been taken from Ref. [30]. The "uncorrelated" refers to the bounds taken from the best among the detector-only and the source-only analyses, while "correlated" refers to the bounds taken from the best among the combined analysis of interplay between the source and detector NSI parameters.

The best amid the bounds in this study are summarized in Table V along with the previous bounds obtained using the similar processes of $\nu_e - e$ and $\overline{\nu}_e - e$ scatterings in Refs. [18–23, 25] and with the indirect bounds of Ref. [30] for comparison.

Acknowledgments

I am very grateful to Professor Douglas McKay of University of Kansas for his continuous encouragement and comments during the course of this work. I also thank Dr. David Forero for the detailed discussions and Dr. Jean-Luc Vuilleumier of MUNU Collaboration for sharing the information and details about the MUNU experiment. This work has been partially supported by the Sun Yat-Sen University under the Post-Doctoral Fellowship program.

[1] Y. Abe *et al*. (Double Chooz Collaboration), Phys. Rev. Lett. **108**, 131801 (2012); Phys. Rev. D **86**, 052008 (2012).
[2] F. An *et al*. (Daya Bay Collaboration), Phys. Rev. Lett. **108**, 171803 (2012); Chin. Phys. C 37, 011001(2013).
[3] J. K. Ahn *et al*. (RENO Collaboration), Phys. Rev. Lett. **108**, 191802 (2012).
[4] Y.-F. Li, "Overview of the Jiangmen Underground Neutrino Detector (JUNO), arXiv:1402.6143v1 [physics.ins-det] (2014).
[5] S. Seo, Introduction to RENO-50, in Proceedings of the International Workshop on RENO-50: Toward Neutrino Mass Hierarchy, Seoul, 2013.
[6] NOvA Collaboration (P. Adamson (Fermilab) *et al*.), FERMILAB-PUB-16-007-ND, [arXiv:1601.05037], Jan 19, 2016. 8 pp.
[7] R. Acciarri *et al*. [DUNE Collaboration], arXiv:1512.06148 [physics.ins-det]; C. Adams *et al*. [LBNE Collaboration], arXiv:1307.7335 [hep-ex],
[8] Neutrino Factory Collaboration (Tracey Li (Durham U., IPPP) for the Collaboration). 2012,
Published in Nucl. Phys. Proc. Suppl. 229-232 (2012) 524.
[9] BOREXINO Collaboration, G. Bellini *et al*., Nature **512** (2014) 383–386, doi, 10.1038/nature13702.
[10] M. Wurm *et al*. [LENA Collaboration], arXiv: [astro-ph,IM] 1104.5620v3.
[11] R.C. Allen, *et al*., Phys. Rev. D **47** (1993) 11.
[12] L.B. Auerbach, *et al*., (LSND Collaboration), Phys. Rev. D **63** (2001) 112001, hep-ex/0101039.
[13] F. Reines, H.S. Gurr, H.W. Sobel, Phys. Rev. Lett. **37** (1976) 315.
[14] G.S. Vidyakin, *et al*., JETP Lett. **55** (1992) 206, Pis'ma Zh. Eksp. Teor. Fiz. **55** (1992) 212.
[15] A. I. Derbin, A.V. Chernyi, L.A. Popeko, V.N. Muratova, G.A. Shishkina, S.I. Bakhlanov, JETP Lett. **57** (1993) 768, Pis'ma Zh. Eksp. Teor. Fiz. **57** (1993) 755.
[16] MUNU [Z. Daraktchieva, *et al*., (MUNU Collaboration), Phys. Lett. B **615** (2005) 153, hep-ex/0502037.
[17] M. Deniz *et al*. (TEXONO Collaboration), Phys. Rev. D **81**, 072001 (2010).
[18] S. Davidson, C. Pena-Garay, N. Rius, and A. Santamaria, J. High Energy Phys. **03**, 011 (2003).
[19] D. V. Forero and M. M. Guzzo, Phys. Rev. D **84**, 013002 (2011).
[20] J. Barranco, O. G. Miranda, C. A. Moura, and J. W. F. Valle, Phys. Rev. D **77**, 093014 (2008).
[21] J. Barranco, O. G. Miranda, C. A. Moura, and J. W. F. Valle, Phys. Rev. D **73**, 113001 (2006).
[22] J. Barranco, O. G. Miranda, T.I. Rashba, Physics Letters B **662** 431–435 (2008).

[23] A. N. Khan, D. W. McKay and F. Tahir, Phys.Rev. D **90**, 053008 (2014), arXiv:1407.4263 [hep-ph].
[24] J. M. Conrad, M. H. Shaevitz, I. Shimizu, J. Spitz, M. Toups and L. Winslow, Phys. Rev. D **89**, 072010 (2014).
[25] M. Deniz *et al*., (TEXONO Collaboration), Phys. Rev. D **82**, 033004 (2010).
[26] A. D. Gouvêa and J. Jenkins, Phys. Rev. D **74**, 033004 (2006).
[27] K. N. Abazajiana *et al*, arXiv:1204.5379v1 [hep-ph] 18 Apr (2012).
[28] Y. Grossman, Phys. Lett. B **359**, 141 (1995).
[29] T. Ohlsson, Rep. Prog. Phys. **76**, 044201 (2013).
[30] C. Biggio, M. Blennow, E. Fernandez–Martinez, JHEP **0908**, 090 (2009).
[31] A. N. Khan, D. W. McKay and F. Tahir, Phys. Rev. D **88**, 113006 (2013), arXiv:1305.4350 [hep-ph].
[32] T. Ohlsson, H. Zhang and S. Zhou, Phys. Lett. B **728**, 148 (2014).
[33] I. Girardi and D. Meloni, Phys. Rev. D **90**, 073011 (2014) , arXiv:1403.5507 [hep-ph] .
[34] I. Girardi, D. Meloni and S. Petcov, Nuclear Physics B **886** (2014) 31-42, arXiv:1405.0416v2 [hep-ph] (2014).
[35] J. Kopp, M. Lindner, T. Ota and J. Sato, Phys. Rev. D **77**, 013007 (2008).
[36] P. Adamson *et al*. (MINOS Collaboration), Phys. Rev. D **88**, 072011 (2013).
[37] L. M. Johnson and D. W. McKay, Phys. Lett. B **433**, 335 (1998).
[38] L. M. Johnson and D. W. McKay, Phys. Rev. D **61**, 113007 (2000).
[39] D. McKay, and L. Johnson, "Probing Lepton Flavor Violation" in Proceedings of PASCOS99, Lake Tahoe, K. Cheung, J. Gunion and S. Mrenna, Eds. World Scientific, Singapore, 2000. pp 204-207.
[40] S. Bergmann and Y. Grossman, Phys. Rev. D **59**, 093005 (1999).
[41] M. C. Gonzalez-Garcia, Y. Grossman, A. Gusso and Y. Nir, Phys. Rev. D **64**, 096006
[42] P. Vogel and J. Engel, Phys. Rev. D **39**, 3378 (1989).
[43] SAGE Collaboration, Phys.Rev. C **80** (2009) 015807
[44] G. Bellini *et al*. (BOREXINO Collaboration), arXiv:1308.0443 [hep-ex], 2 Aug. 2013.